AMERICAN ACADEMY OF OPHTHALMOLOGY®

Characterization of Ultra-Widefield Angiographic Vascular Features in Diabetic Retinopathy with Automated Severity Classification

Duriye Damla Sevgi, MD,[1] Sunil K. Srivastava, MD,[1] Jon Whitney, PhD,[1] Margaret O'Connell, BSc,[1] Sudeshna Sil Kar, PhD,[1,2] Ming Hu, PhD,[1,3] Jamie Reese, BSN,[1] Anant Madabhushi, PhD,[2] Justis P. Ehlers, MD[1]

Purpose: To determine the association between diabetic retinopathy (DR) severity and quantitative retinal vascular features.

Design: Retrospective image analysis study.

Participants: Eyes with DR and eyes with no posterior segment disease (normal eyes) that had undergone ultra-widefield fluorescein angiography (UWFA) with associated color fundus photography. Exclusion criteria were any previous laser photocoagulation, low image quality, intravitreal or periocular pharmacotherapy within 6 months of imaging, and any other significant retinal disease including posterior uveitis, retinal vein occlusion, and choroidal neovascularization.

Methods: The centered early mid-phase UWFA frame that captured the maximum vessel area was selected using automated custom software for each eye. Panretinal and zonal vascular features were extracted using a machine learning algorithm. Eyes with DR were graded for DR severity as mild nonproliferative DR (NPDR), moderate NPDR, severe NPDR, and proliferative DR (PDR). Parameters of normal eyes were compared with age- and gender-matched patients with DR using the *t* test. Differences between severity groups were evaluated by the analysis of variance and Kruskal-Wallis tests, generalized linear mixed-effects models, and random forest regression models.

Main Outcome Measures: Diabetic retinopathy severity and vascular features (panretinal and zonal vessel area, length and geodesic distance, panretinal area index, tortuosity measures, vascular density measures, and zero vessel density rate).

Results: Ninety-seven eyes from 60 patients with DR and 12 normal eyes from 12 patients that underwent UWFA for evaluation of fellow eye pathology had images of sufficient quality to be included in this analysis. The mean age was 60 $\pm$ 10 years in DR eyes and 46 $\pm$ 17 years in normal eyes. Panretinal vessel area, mean geodesic distance, skewness, and kurtosis of local vessel density was significantly higher in normal eyes compared with the age- and gender-matched eyes with DR ($P < 0.05$). Zero vessel density rate, skewness of vessel density, and mean mid-peripheral geodesic distance were among the most important features for distinguishing mild NPDR from advanced forms of DR and PDR versus eyes without PDR.

Conclusions: Automated analysis of retinal vasculature demonstrated associations with DR severity and visual and subvisual vascular biomarkers. Further studies are needed to evaluate the clinical significance of these parameters for DR prognosis and therapeutic response. *Ophthalmology Science 2021;1:100049* © *2021 by the American Academy of Ophthalmology. This is an open access article under the CC BY-NC-ND license (http://creativecommons.org/licenses/by-nc-nd/4.0/).*

The prevalence of diabetes mellitus in the United States in 2018 was estimated to be 13% of the adult population, corresponding to 34.1 million patients.[1] Diabetic retinopathy (DR), the most common complication of uncontrolled diabetes mellitus, remains one of the leading causes of legal blindness worldwide.[2] Microvascular changes are vital to the diagnosis and staging of DR, as outlined in the guidelines suggested by the Early Treatment Diabetic Retinopathy Study group.[3,4] The development of ultra-widefield fluorescein angiography (UWFA) allows these microvascular changes to be visualized and measured panretinally and has become a primary tool for DR diagnosis.[5,6] Ultra-widefield fluorescein angiography facilitated the quantification of clinically used imaging features such as nonperfusion and leakage and introduced new angiographic biomarkers such as retinal vessel area, tortuosity, vascular fractal dimension (branch complexity), vascular geodesic distance (the shortest distance between 2 points in a given shape), and leakage distribution features.[7–13]

Quantitative assessment of fluorescein angiographic features in DR is limited in the current literature. Previous

https://doi.org/10.1016/j.xops.2021.100049
ISSN 2666-9145/21

studies have demonstrated an association between panretinal leakage index, panretinal ischemic index, and panretinal microaneurysm and DR severity.[11] Fan et al[7] found that the fractal dimension indicating branching complexity of the peripheral retinal vasculature was decreased compared with that of normal eyes and correlated with ischemia in eyes with DR.

Deep learning algorithms provide opportunities for advanced segmentation of imaging features, including retinal vasculature extraction from UWFA frames.[7,8,12–15] Following deep learning-based vascular segmentation, this study evaluated the association between DR severity and quantitative panretinal vascular features, including vessel area, geodesic distance, tortuosity measures, and vessel density measures. Quantification of these features may allow for better understanding of the vasculopathy, disease activity, and risk factors of DR progression.

Methods

Study Population

In this institutional review board-approved retrospective image analysis study, patients with DR and those with no posterior segment disease (normal eyes) who had undergone UWFA imaging with the California (Optos) system and concurrent color fundus photography were identified. The Cleveland Clinic Investigational Review Board approved the study, which adhered to the tenets of the Declaration of Helsinki. Because of the retrospective nature of the study, informed consent was not required. Exclusion criteria were any previous laser photocoagulation, intravitreal or periocular pharmacotherapy within 6 months of imaging, and any other significant retinal disease including posterior uveitis, retinal vein occlusion, and choroidal neovascularization. In addition, eyes with images of insufficient quality for detailed retinal vasculature extraction such as poor contrast, increased background hyperfluorescence, media opacity and artifacts obstructing the view, and defocused areas were excluded, as outlined below. Eyes with minimal media opacities were included at the grader's discretion based on the opacity's impact on the vessel segmentation. Eyes with DR were graded for DR severity as mild nonproliferative DR (NPDR), moderate NPDR, severe NPDR, and proliferative DR (PDR) based on the International Clinical Diabetic Retinopathy Disease Severity Scale (DRSS) using the concurrent fundus photograph by a trained grader. The DRSS grades were reviewed sequentially by a senior image analyst, and any discrepancies were adjudicated by the senior author (J.P.E.).

Automated Image Selection

A previously described automated image selection tool was used to select the optimal early-phase image with the widest visualization of retinal vasculature.[14] In brief, the retinal vasculature was extracted from all frames of an angiographic session using a deep learning algorithm. The frame with maximum retinal vessel area was identified as the optimal arteriovenous phase image. Among the frames with later than a 4-minute timestamp, the image with retinal vessel area closest to that of arteriovenous phase was selected as the optimal late image. Automated selections were reviewed for the field of view errors and replaced with a more centered image when needed per the image analyst's discretion. Optic disc location was used to determine the centration of the image. Images with optic discs located within ±550 pixel range on temporonasal axis and ±350 pixel range on the superoinferior axis from the center of the image were considered centered. Sufficient image quality for vasculature analysis was assessed based on the contrast of the image, media opacity and artifacts obstructing the view, defocused retina, and microvasculature details in the extracted retinal vasculature mask. Images with insufficient quality resulting in suboptimal vessel segmentations were excluded. Images with minimal opacities that resulted in minor segmentation defects were not excluded. Images were corrected by a previously described dewarping transformation software, which enabled pixel-to-millimeter conversion of the vascular area parameters.[16] A region of interest for each image was determined by a trained image analyst (D.D.S.) capturing the visible vasculature excluding artifacts caused by eyelids and eyelashes (Fig 1). A qualitative review of regions of interest was performed after the vascular segmentations were extracted to ensure that no significant defects were caused by imaging artifacts. Regions of interest with major defects were modified as needed before vascular parameter extraction.

Vascular Parameter Extraction

As previously described, an automated quantitative angiographic assessment tool with deep-learning augmentation was used to segment and evaluate angiographic features.[10,13,14] Vascular parameters, including panretinal and zonal vessel area and length, panretinal area index, panretinal and zonal geodesic distance, panretinal tortuosity measures (mean, median, variance, skewness, and kurtosis), and panretinal vascular density measures (mean, median, variance, skewness, kurtosis, and zero vessel density rate) were calculated using custom Python and MATLAB scripts. The zonal assessment was performed for vessel area and geodesic distance parameters in 2 fovea-centered regions shown in Figure 2. Macular zone was defined as the circular area of 40 mm^2 (approximately 5 optic disc areas) with a 3.6-mm radius (200 pixels), and the mid-peripheral zone was defined as the donut-shaped region between circular areas with a 3.6-mm radius and 11.1-mm radius (200 and 750 pixels).

A previously available tool (Morpholib Image J) was used to create disc centered geodesic distance maps from vessel masks.[17] The geodesic distance was defined as the shortest distance from the center of the optic disc while staying inside extracted vessel masks to the final point of interest. The mean geodesic distance was the average of geodesic distances from all pixels that make the vascular mask. The maximum geodesic distance was the distance from the center of the optic disc to the end point on the longest vascular branch (Fig 3).

Two additional novel parameters were calculated: (1) vessel area index and (2) localized vessel density. Vessel area index was defined as the percentage of detectable retinal vasculature in the retinal region of interest. It was calculated by dividing the retinal vessel area by the total area of the region of interest. Localized vessel density was assessed to investigate the distribution of retinal vessel density, and the extracted panretinal vasculature mask was divided into 40 × 40-pixel squares (Fig 3). Percentages of the areas occupied with retinal vessels were calculated for each square, and these values were used to compute the mean, median, variance, skewness, and kurtosis values of localized retinal vessel density across the panretinal area. The zero vascular density rate was calculated as the ratio of squares with vessel density less than 5% in the entire region of interest, after a neighbor square vessel density-based artifact removal. If all the neighbors of a square with less than 5% vessel occupancy showed vessel presence of more than 5%, the vessel density value of the middle square was replaced by the mean of its neighbors.

The methods for measuring vascular tortuosity have been described previously.[9] A summary of these steps for calculating

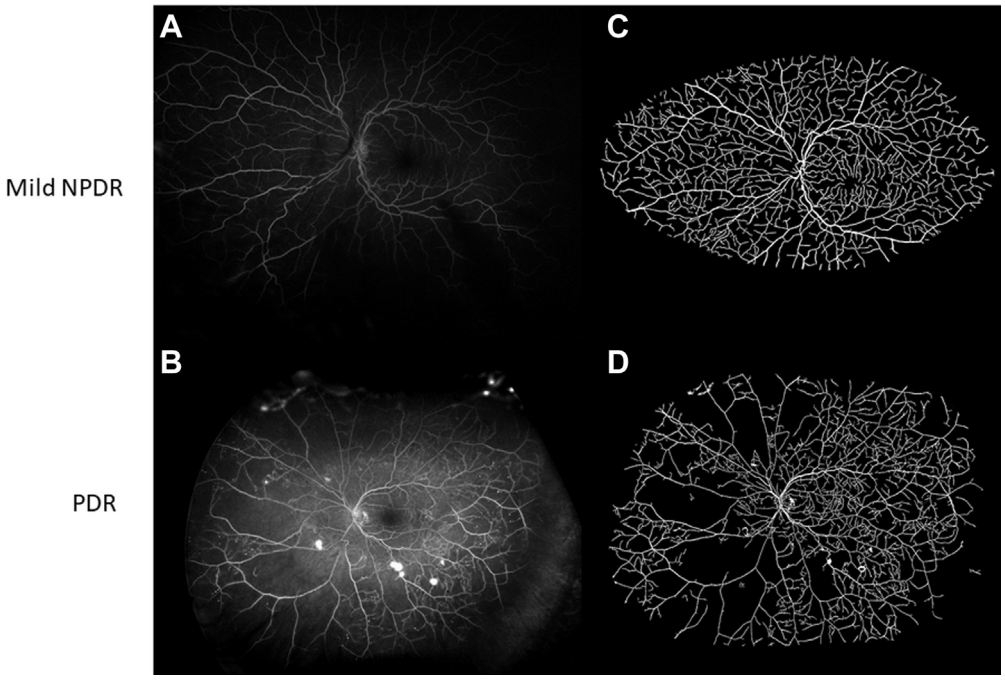

Figure 1. Vascular map extraction: ultra-widefield fluorescein angiography examples of eyes with (**A**) nonproliferative diabetic retinopathy (NPDR) and (**B**) proliferative diabetic retinopathy (PDR), and (**C**, **D**) their respective corresponding deep learning-based vasculature segmentation demonstrating diabetic retinopathy's vascular abnormalities in the expert-determined region of interest.

vascularity tortuosity are as follows: first the vessel center lines are computed, and a series of points S are generated in 3-dimensional Cartesian space, which comprises the medial axis skeleton of the vessels. S is projected along the plane of image acquisition, z, and a 2-dimensional representation of the vasculature, V_{xy}, is obtained. This depicts the vascular network in the xy-plane. The tortuosity features consist of the first-order statistics (mean, median, variance, skewness, and kurtosis) of maximum Hough peak orientations computed in a sliding fashion across vessel projections summarizing vasculature orientation in the xy-plane.

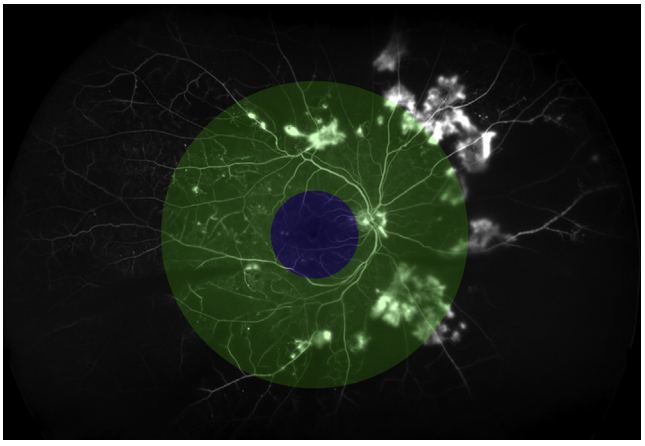

Figure 2. Zonal assessment: the macular zone (blue) is the circular area of 40 mm^2 (approximately 5 optic disc areas) with a 3.6-mm radius (200 pixels), and the mid-peripheral zone (green) is the donut-shaped region between circular areas with a 3.6-mm radius and a 11.1-mm radius (200 and 750 pixels).

Statistical Analysis

All statistical analyses were performed using R software version 3.6.1 (R Foundation for Statistical Computing). Distribution of normality of the continuous variables was assessed using the Shapiro-Wilk normality test. Parameters of normal eyes were compared with those of age- and gender-matched patients with DR using the t test. Differences between groups (normal, mild NPDR, moderate NPDR, severe NPDR, and PDR) were evaluated by the analysis of variance and Kruskal-Wallis tests for parametric and nonparametric parameters, respectively. Generalized linear mixed-effect modeling was used to compare groups—normal versus mild NPDR, PDR versus non-PDR (mild NPDR, moderate NPDR, and severe NPDR), mild NPDR and moderate NPDR versus severe NPDR and PDR, and mild NPDR versus moderate or worse DR (moderate NPDR, severe NPDR, and PDR)—while considering intereye correlation. A P value of less than 0.05 was considered statistically significant. Random forest regression models grown with 1000 trees in 5-fold cross-validated settings using randomly selected 80% of the data for training and 20% for testing were used to determine the most important features for normal versus mild NPDR, normal and mild NPDR versus advanced DR (i.e., moderate NPDR, severe NPDR, and PDR), PDR versus non-PDR, and normal versus severe NPDR and PDR differentiation.

Results

Demographics and Clinical Features

Ninety-seven eyes from 60 patients with DR and 12 normal eyes from 12 patients had images of sufficient quality to be included in the study. Fifteen images (13.7 %) showed with minimal media opacities (1 normal, 3 mild NPDR, 3

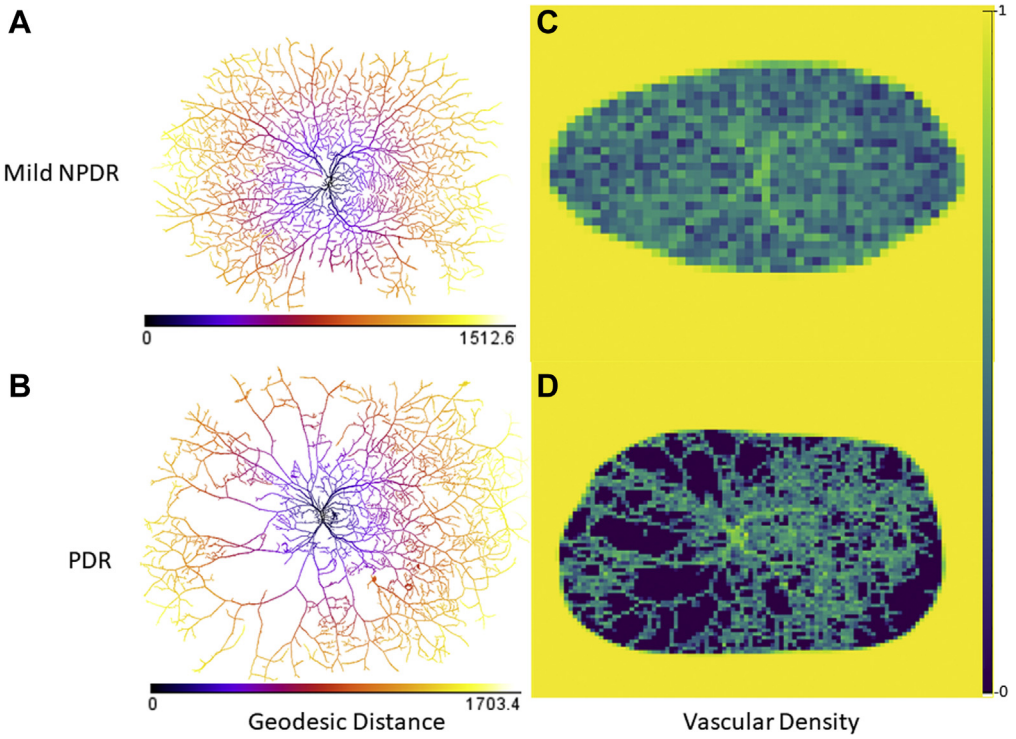

Figure 3. Geodesic distance and localized vessel density map examples of eyes with (**A**) nonproliferative diabetic retinopathy (NPDR) and (**B**) proliferative diabetic retinopathy (PDR). The optic disc center was used as the reference point to create the geodesic distance maps. The color scale demonstrates the change from cold colors to warm colors as the geodesic distance increases in pixels. In localized vessel density maps of the eyes with (**C**) NPDR and (**D**) PDR, zero vessel density areas are represented in purple, as demonstrated in the color scale. Yellow areas are excluded from the analysis using expert-determined regions of interest.

moderate NPDR, 4 severe NPDR, and 4 PDR). The mean age was 60 ± 10 years in DR eyes and 46 ± 17 years in normal eyes. In the DR sample, gender distribution of patients and eyes included were 39 men (65%), 60 eyes (62%) from men, 21 women (35%), and 37 eyes from women (38%). The normal sample included 6 men and 6 women. Sixteen eyes had mild NPDR, 25 eyes had moderate NPDR, 33 eyes had severe NPDR, and 23 eyes had PDR. Demographics in each DR severity and normal category are summarized in Table 1. In evaluating the consistency of the region of interest size, the mean maximum edge-to-edge distance was 2321 ± 171 pixels in normal eyes, 2383 ± 309 pixels in mild NPDR eyes, 2194 ± 273 pixels in moderate NPDR eyes, 2156 ± 270 pixels in severe NPDR eyes, and 2413 ± 289 pixels in PDR eyes. No significant differences were found between the maximum edge-to-edge distance between the groups.

Comparison of Normal Retinal Vasculature and Diabetic Retinopathy Vasculature

Age and gender were matched in 10 normal eyes and 10 eyes with DR. Mean age was 50 ± 16 years. Three eyes had mild NPDR, 1 eye had moderate NPDR, 4 eyes had severe NPDR, and 2 eyes had PDR. Panretinal vessel area was significantly higher in normal eyes (91.1 ± 9.2 mm^2) compared with eyes with DR (76.7 ± 15.3 mm^2; P = 0.022). No significant differences were found in the macular vessel area between the normal eyes (7.5 ± 0.7 mm^2) and eyes with DR (7.1 ± 0.7 mm^2). Panretinal geodesic mean was significantly higher in normal eyes (784 ± 64 pixels) compared with eyes with DR (695 ± 101 pixels; P = 0.033). Variance (P = 0.032) of localized vessel density was significantly lower in normal eyes, whereas skewness (P = 0.006) and kurtosis (P = 0.005) were higher. The zero vessel density rate was significantly higher in DR eyes (11.3 ± 10.4 %) compared with that of normal eyes (0.6 ± 0.5 %; P = 0.010; Table 2).

Early Vascular Changes in Diabetic Retinopathy and Automated Identification of Early Diabetic Retinopathy

Mean panretinal vessel area was significantly greater in normal eyes (90.7 ± 10.5 mm^2) compared with eyes with mild NPDR (70.8 ± 16.2 mm^2; P = 0.003; Table 3). Macular vessel area (P = 0.042) and mid-peripheral vessel area (P < 0.001) also were decreased significantly in eyes with mild NPDR. Panretinal geodesic maximum (P < 0.001) and mean mid-peripheral geodesic distance (P = 0.011) were significantly greater in normal eyes. Variance of tortuosity was significantly higher (P < 0.001) in eyes with mild NPDR (108.9 ± 1.5) compared with normal eyes (107.6 ± 1.8). Panretinal variance of localized vessel density was significantly lower in normal eyes (2.8 ± 0.2%) compared with eyes with mild NPDR (3.2 ± 0.4%;

Table 1. Demographics of Patients and Eyes Included in Each Severity Group

Variable	Normal	Nonproliferative Diabetic Retinopathy			Proliferative Diabetic Retinopathy
		Mild	*Moderate*	*Severe*	
Age (yrs)	46 ± 17	61 ± 17	66 ± 6	58 ± 12	56 ± 7
Eyes					
Male	6	9	13	18	16
Female	6	7	12	15	7
Patients					
Male	6	7	9	15	12
Female	6	4	8	10	5

Data are presented as no. or mean ± standard deviation.

$P < 0.001$). Zero vessel density rate was significantly higher in mild NPDR (6.9 ± 9.6%) compared with normal eyes (0.5 ± 0.5%; $P = 0.025$). Skewness ($P < 0.001$) and kurtosis ($P < 0.001$) of localized vessel density was significantly higher in eyes with normal vasculature.

Random forest classification ran in a 3-fold cross-validated setting demonstrated an area under the receiver operating characteristics curve (AUC) of 0.81 ± 0.16 for distinguishing between normal eyes and mild NPDR eyes. The top 5 most discriminating features included variance, skewness of localized vessel density, kurtosis of localized vessel density, kurtosis of vessel tortuosity, and panretinal vessel area.

Vascular Features of Diabetic Retinopathy Severity

Panretinal vessel area oscillated with the progression of DR, with the mean increasing from mild NPDR (70.8 ± 16.2 mm^2) to moderate NPDR (73.4 ± 18.9 mm^2) and decreasing at severe NPDR (76.0 ± 20 mm^2) and increasing at PDR (88.3 ± 22.7 mm^2; $P = 0.034$; Table 3). The same pattern was observed in the mid-peripheral zone ($P = 0.041$). Retinal vessel area in the macular zone trended toward lower values in PDR eyes (6.6 ± 1.5 mm^2) compared with eyes with mild NPDR (6.9 ± 0.6 mm^2), moderate NPDR (7.0 ± 1.0 mm^2), and severe NPDR (7.0 ± 1.4 mm^2); however, this result was not significant ($P = 0.513$). Mean geodesic distance was increased in eyes with PDR panretinally ($P = 0.006$) and in the mid-peripheral zone ($P < 0.001$). Skewness of localized vascular density (mild NPDR, 2.771 ± 0.266; moderate NPDR, 2.768 ± 0.186; severe NPDR, 2.679 ± 0.185; and PDR, 2.553 ± 0.139; $P < 0.001$) was significantly lower in PDR compared with NPDR categories. In addition, the zero vascular density rate (mild NPDR, 6.9 ± 9.5%; moderate NPDR, 6.9 ± 9.2%; severe NPDR, 8.2 ± 9.3%; and PDR, 18.6 ± 10.4%; $P < 0.001$) was significantly higher in PDR and trended toward an increase in the severe NPDR group. Skewness of localized vessel density ($P = 0.014$) was significantly higher and zero value density rate ($P = 0.048$) was significantly lower in early (mild NPDR and moderate NPDR) stages of DR compared with the late stages (severe NPDR and PDR). Significantly higher macular vessel area ($P < 0.001$), higher mean tortuosity ($P < 0.001$), lower skewness of tortuosity ($P < 0.001$), and higher variance of vessel density ($P < 0.001$) was found when mild NPDR was compared with more advanced disease (moderate NPDR, severe NPDR, and PDR; Fig 4).

The random forest classifier achieved an AUC of 0.84 ± 0.15 for distinguishing eyes with PDR versus those with NPDR. The top 5 distinguishing features were zero vessel density rate, skewness of localized vessel density, mid-peripheral vessel area, mean mid-peripheral geodesic distance, and panretinal mean geodesic distance. The top 5 features distinguishing mild NPDR from advanced forms of the disease were skewness and variance of localized vessel density, kurtosis of vessel tortuosity, zero vessel density, and panretinal mean geodesic distance for the random forest classifier with an AUC of 0.61 ± 0.13. An AUC of 0.95 ± 0.05 was achieved for distinguishing normal eyes and eyes with severe NPDR or PDR, with the 2 primary distinguishing features between DR severity classes being the skewness of localized vessel density and zero vessel density rate.

Discussion

In this study, we investigated the association between vascular features extracted from UWFA images with DR severity. Using the widefield visualization advantage of UWFA, we performed panretinal and zonal assessment of the retinal vessel area, geodesic distance, tortuosity, and vessel density. Several vascular parameters were significantly different in normal eyes compared with the age- and gender-matched eyes with DR. Decrease in panretinal vessel area, decrease in panretinal mean geodesic distance, increase in variance of density, and decrease in skewness and kurtosis of vessel density were demonstrated to be early changes in vasculature in the setting of DR. Tortuosity features and vessel density features were found to be significantly different in mild NPDR compared with the later stages of DR. Zero vessel density rate, skewness of vessel density, and mean mid-peripheral geodesic distance were identified as promising biomarkers for automated classification.

The interest in quantitative analysis of retinal vasculature has grown with the development of OCT angiography (OCTA), which provides visualization of multiple layers of

Table 2. Statistically Significant Differences in Vascular Parameters between Age- and Gender-Matched Normal Eyes and Eyes with Diabetic Retinopathy

Vascular Feature	Normal Eyes (n = 10)	Eyes with Diabetic Retinopathy (n = 10)	*P* Value*
Panretinal vessel area (mm^2)	91.1 ± 9.2	76.7 ± 15.3	0.022
Panretinal mean geodesic distance (pixels)	784 ± 64	695 ± 101	0.033
Variance of localized vessel density (%)	2.81 ± 0.2	3.19 ± 0.3	0.032
Skewness of localized vessel density	3.00 ± 0.08	2.72 ± 0.21	0.006
Kurtosis of localized vessel density	10.0 ± 0.7	8.2 ± 1.4	0.005
Zero vessel density (%)	0.6 ± 0.5	11.3 ± 10.4	0.010

*Calculated using the *t* test. $P < 0.05$ was considered statistically significant.

retinal vasculature in the macular region. Diabetic retinopathy is a unique disease that demonstrates itself with both microvascular loss and remodeling. This introduces challenges in using vascular features such as retinal vessel area for analysis. The vessel extraction method used in this study provided detailed vessel masks for higher-order assessment. We recently demonstrated that detected vasculature is highly phase sensitive, especially in the earlier phases of angiography; therefore, an automated image selection method was used to select the most detailed mask.[14] In addition to the macular zone traditionally scanned with OCTA, the mid and far periphery were assessed for vascular differences associated with DR severity.

The mean vessel area increased from mild NPDR to moderate NPDR, decreased with severe NPDR, and increased with PDR. This may be evidence of an oscillating pattern in panretinal vessel area with the progression of DR. Vascular density analysis using 60° fluorescein angiography images demonstrated the same oscillating pattern from NPDR to PDR.[18] The oscillation was attributed to the capacity of recovery in earlier stages of retinopathy. It is hypothesized that a multifactorial process mediates the oscillating pattern with competing stimulatory and inhibitory factors such as hypoxia and vascular endothelial growth factor production.[18] In our study, the mid-peripheral zones followed the same pattern. However, in the macular zone, eyes with PDR demonstrated a trend of decreased vessel area. This finding is concordant with previous OCTA studies showing decreased vascular density in eyes with PDR compared with those with NPDR.[19,20] Further studies investigating the relationship of vascular remodeling locations with ischemic lesions and their physiological underpinnings, including biological markers such as cytokines, are needed to understand better the discrepancy in vascular area change between the macular zone and the periphery as the DR progress.

In a previous study that quantified vascular parameters using UWFA images, the mean vascular bed area in normal patients was found to be 42.3 ± 14.8 mm^2.[8] The mean vessel area of normal eyes in our dataset was 91.1 ± 9.2 mm^2. Compared with conventional image processing techniques, the superior detail capture of convoluted deep learning algorithms and automated selection of the most detailed vessel mask may account for the difference.[14] Panretinal vessel area in eyes with DR was decreased compared with normal eyes in our dataset. Vessel masks successfully extracted DR's vascular abnormalities, including vascular occlusions, intraretinal microvascular abnormalities (IRMA), and neovascularization in detail (Fig 1).

Tortuosity features, including mean tortuosity and skewness of tortuosity, were found to be significantly different in mild NPDR compared with later DR stages. In an OCTA study, superficial retinal layer tortuosity was found to increase with DR severity in NPDR and to decrease in PDR.[21] We demonstrated a trend of reduced tortuosity in PDR compared with mild and moderate NPDR. A previous OCTA study quantifying tortuosity changes in areas

Table 3. Summary of the Means and Standard Deviations of the Select Vascular Features in Normal Eyes and Diabetic Severity Groups

Vascular Features	Normal	Nonproliferative Diabetic Retinopathy			Proliferative Diabetic Retinopathy	*P* Value*
		Mild	*Moderate*	*Severe*		
Panretinal vessel area (mm^2)	90.7 ± 10.5	70.8 ±16.2	73.4 ± 18.9	76.0 ± 20.0	88.3 ± 22.7	0.003
Macular vessel area (mm^2)	7.4 ± 0.7	6.9 ± 0.6	7.0 ± 1.0	7.0 ± 1.4	6.6 ± 1.5	0.097
Panretinal mean geodesic distance (pixels)	795 ± 68	716 ± 116	689 ± 94	687 ± 87	775 ± 92	< 0.001
Mean of localized vessel density (%)	18.9 ± 1.2	19.7 ± 2.1	19.4 ± 2.0	20.3 ± 2.6	19.0 ± 3.0	0.246
Skewness of localized vessel density	2.995 ± 0.095	2.771 ± 0.266	2.768 ± 0.186	2.679 ± 0.185	2.553 ± 0.139	< 0.001
Kurtosis of localized vessel density	9.980 ± 0.672	8.247 ± 1.750	8.316 ± 1.504	7.884 ± 1.200	8.0367 ± 0.769	< 0.001
Mean vascular tortuosity	165 ± 3	166 ± 2	166 ± 3	165 ± 3	165 ± 3	0.546
Zero vessel density (%)	0.5 ± 0.5	6.9 ± 9.5	6.9 ± 9.2	8.2 ± 9.3	18.6 ± 10.4	< 0.001

*Evaluated by the analysis of variance and Kruskal-Wallis tests for parametric and nonparametric parameters, respectively. $P < 0.05$ was considered statistically significant.

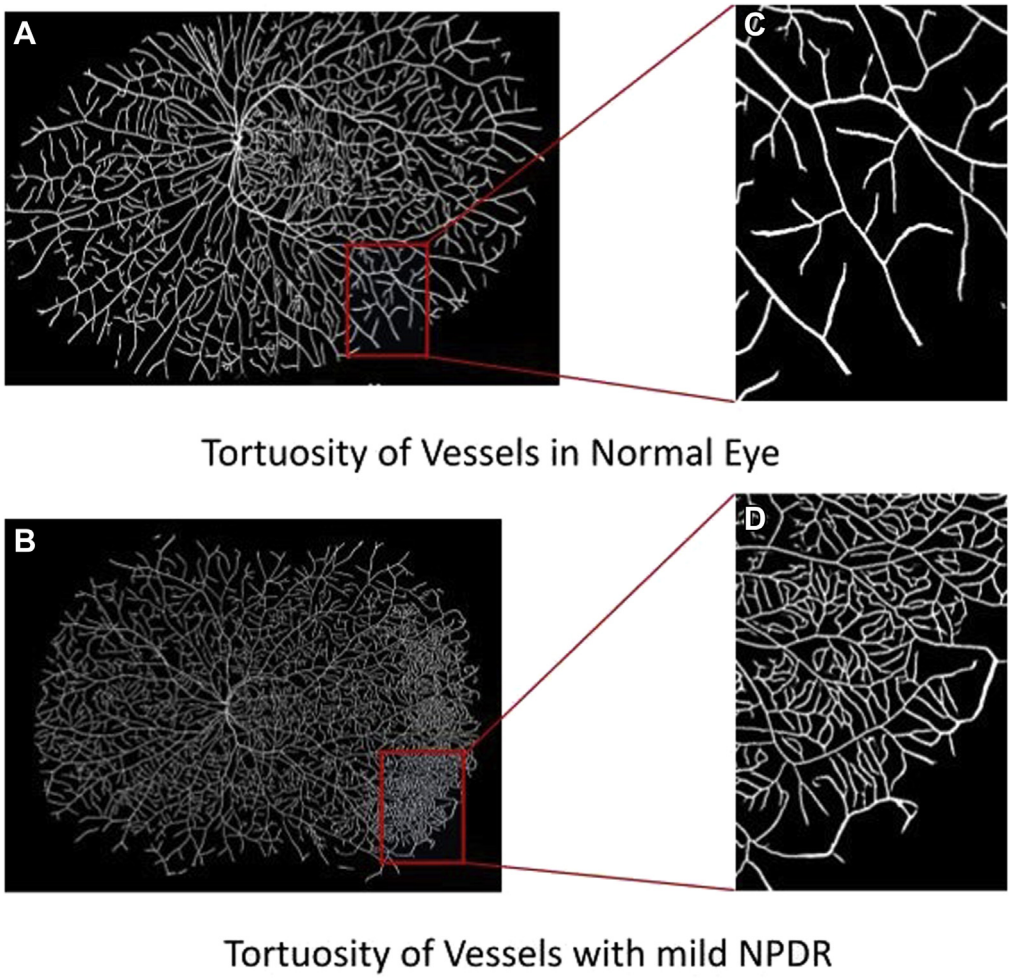

Figure 4. **A**, **B**, Vessel mask examples of (**A**) a normal eye and (**B**) an eye with mild NPDR demonstrating the higher variance of tortuosity in the eye with mild nonproliferative diabetic retinopathy (NPDR) compared with the normal eye. **C**, **D**, Close-up view of the areas enclosed by the red square in the vessel masks of the normal eye and the eye with mild NPDR, respectively.

centered on optic disc with 3 mm and 1.5 mm radii suggested that the tortuous changes were disseminated from center to periphery in DR.[21] Zonal assessment of tortuosity features could provide more insight into the pathogenesis of tortuosity. A color fundus photograph study demonstrated that arteriolar tortuosity was associated with mild and moderate levels of DR, whereas venular tortuosity was not associated with DR severity.[22] Vascular masks extracted from UWFA images did not differentiate between arteries and veins. The decreased tortuosity measured in severe NPDR and PDR might be explained by the reduction of transmural pressure as DR progresses to severe nonproliferative and proliferative stages.[23] Another contributing factor to the decreased mean tortuosity measures in severe NPDR and PDR may be vascular sclerosis. The vascular loss may skew the tortuosity measures to higher means.

Geodesic distance, defined as the shortest distance between two points in a given shape, has been used in quantitative studies in other areas of medicine.[24,25] Mean geodesic distance is a unique biomarker in DR because it accounts for vascular loss or remodeling location. Thus, it may be a more sensitive biomarker than the vessel area. Distal vascular loss and increased vessel area proximally resulting from venous beading or tortuosity would decrease the mean geodesic distance. In contrast, distal remodeling such as IRMA would increase it. The mean panretinal and mid-peripheral geodesic distance were among the top 5 most discriminating features between PDR and NPDR. These findings can be explained by vascular remodeling such as IRMA and proliferative changes such as neovascularization elsewhere (NVE). Increased mean geodesic biomarker can be a more sensitive late-stage disease biomarker compared with the vessel area or density. Further studies are needed to explore its associations with progression and treatment response.

As part of this assessment, we developed a novel assessment for nonperfusion based on a localized vascular density measure for UWFA. The vascular density was calculated throughout the region of interest using 40 × 40-pixel squares. Panretinal mean vascular density was not different across the different DR severity groups. In

advanced stages of DR, areas of vascular dropout and angiogenesis were observed simultaneously. These changes, contributing in different directions to the vascular density measures, may eliminate their effect in mean calculations. In addition, vascular loss and remodeling may provide greater contrast, in turn enabling visualization of individual vessels, which may confound mean calculations even further. Therefore, features taking account of the distribution of the vascular density may be more sensitive biomarkers than the mean vascular density for panretinal assessment. We demonstrated that variance and skewness of density measures were associated with earlier stages of DR. Zero vascular density metrics were created after a skewness of density-based artifact removal. This feature demonstrated a similar trend observed in ischemia index changes with DR severity. The correlation between zero vascular density metrics and ischemia index should be investigated further to explore this biomarker's potential as an automated alternative to the ischemia index.

This study has several limitations, including its retrospective design. A specific UWFA imaging protocol was not followed. Although an automated image selection method was used to ensure a standard on the extracted vasculature detail among the participants, the effects of other factors such as contrast and focus were not excluded fully. Axial length measurements of the patients were not available. Pixel-to-square millimeter conversions were not adjusted to actual axial length. Zonal assessment, which could provide more insight on pathogenesis, was not performed for tortuosity and vascular density features. This study did not evaluate the effect of the clinical factors such as age, gender, hemoglobin A1c levels, smoking status, and comorbidities on the vascular features. For image grading, including DRSS and angiographic image selection, a sequential approach for image assessment was used without dual parallel readers and without the ability to calculate intraclass correlation between readers. However, for angiographic selection, an automated objective tool for initial image selection provides an important standardized foundation. In addition, use of the clinical DRSS rather than the Early Treatment Diabetic Retinopathy Study DRSS scale provides less variability and complexity in image scoring. Despite these limitations, we identified novel angiographic biomarkers associated with DR severity. Future analyses are needed with independent datasets for further validation.

We identified associations with DR severity and visual and subvisual vascular biomarkers with the automated analysis of retinal vasculature. Further studies are needed to evaluate the clinical significance of these parameters for DR prognosis and therapeutic response. With prospective studies, quantitative angiographic biomarkers may help to improve treatment decisions, prognosis predictions, screening, and staging guidelines.

Footnotes and Disclosures

Originally received: March 16, 2021.
Final revision: July 20, 2021.
Accepted: July 26, 2021.
Available online: July 30, 2021. Manuscript no. D-21-00043.

[1] The Tony and Leona Campane Center for Excellence in Image-Guided Surgery and Advanced Imaging Research, Cole Eye Institute, Cleveland Clinic, Cleveland, Ohio.

[2] Department of Biomedical Engineering, Case Western Reserve University, Cleveland, Ohio.

[3] Department of Quantitative Health Sciences, Lerner Research Institute, Cleveland Clinic, Cleveland, Ohio.

Disclosure(s):

All authors have completed and submitted the ICMJE disclosures form.

The author(s) have made the following disclosure(s): S.K.S.: Financial support − Regeneron, Allergan, Gilead; Consultant − Bausch & Lomb, Novartis, Regeneron.

A.M.: Financial support − AstraZeneca, Bristol Myers-Squibb, Philips; Equity owner − Inspirata, Inc, Elucid Bioimaging; Consultant − Aiforia

J.P.E.: Financial support − Aerpio, Alcon, Thrombogenics/Oxurion, Regeneron, Genentech, Novartis, Allergan; Consultant − Aerpio, Adverum, Alcon, Allegro, Allergan, Genentech/Roche, Stealth, Novartis, Thrombogenics/Oxurion, Leica, Zeiss, Regeneron, Santen; Patent − Leica

Supported by Research to Prevent Blindness, Inc., New York, New York; Cole Eye Institute, Cleveland, Ohio (institutional grant); the National Eye Institute, National Institutes of Health, Bethesda, Maryland (grant no.: K23-EY022947); and the Betty J. Powers Retina Research Fellowship.

HUMAN SUBJECTS: Human subjects were included in this retrospective study. The human ethics committees at Cleveland Clinic approved the retrospective study. All research adhered to the tenets of the Declaration of Helsinki. Because of the retrospective nature of the study, informed consent was not required.

No animal subjects were included in this study.

Author Contributions:

Conception and design: Ehlers

Analysis and interpretation: Sevgi, Srivastava, Whitney, Kar, Hu, Reese, Madabhushi, Ehlers

Data collection: Sevgi, Whitney, O'Connell, Reese, Madabhushi, Ehlers

Obtained funding: N/A; Study was performed as part of the authors' regular employment duties. No additional funding was provided.

Overall responsibility: Sevgi, Srivastava, Whitney, O'Connell, Kar, Hu, Reese, Madabhushi, Ehlers

Abbreviations and Acronyms:
AUC = area under the receiver operating characteristics curve; **DR** = diabetic retinopathy; **UWFA** = ultra-widefield fluorescein angiography; **DRSS** = diabetic retinopathy severity scale; **IRMA** = intraretinal microvascular abnormalities; **NPDR** = nonproliferative diabetic retinopathy; **NVE** = neovascularization elsewhere; **OCTA** = OCT angiography; **PDR** = proliferative diabetic retinopathy.

Keywords:
Diabetic retinopathy, Quantitative ultra-widefield angiography, Retinal vessel area, Tortuosity.

Correspondence:
Justis P. Ehlers, MD, Cole Eye Institute, Cleveland Clinic, 9500 Euclid Ave, i32, Cleveland, OH 44195. E-mail: ehlersj@ccf.org.

References

1. Centers for Disease Control and Prevention. National Diabetes Statistics Report, 2020. Atlanta, GA: Centers for Disease Control and Prevention, U.S. Dept of Health and Human Services; 2020.
2. Universal eye health: a global action plan 2014-2019. In: WHO Library Cataloguing-in-Publication Data. Geneva, Switzerland: World Health Organization 2013. https://www.who.int/blindness/AP2014_19_English.pdf. Accessed August 13, 2021.
3. Wilkinson CP, Ferris 3rd FL, Klein RE, et al. Proposed international clinical diabetic retinopathy and diabetic macular edema disease severity scales. *Ophthalmology*. 2003;110(9):1677−1682.
4. Early Treatment Diabetic Retinopathy Study Research Group. Grading diabetic retinopathy from stereoscopic color fundus photographs—an extension of the modified Airlie House classification: ETDRS report number 10. *Ophthalmology*. 2020;127(4S):S99−S119.
5. Manivannan A, Plskova J, Farrow A, et al. Ultra-wide-field fluorescein angiography of the ocular fundus. *Am J Ophthalmol*. 2005;140(3):525−527.
6. Han IC, Zhang AY, Liu TYA, et al. Utility of ultra-widefield retinal imaging for the staging and management of sickle cell retinopathy. *Retina*. 2019;39(5):836−843.
7. Fan W, Nittala MG, Fleming A, et al. Relationship between retinal fractal dimension and non-perfusion in diabetic retinopathy on ultra-wide field fluorescein angiography. *Am J Ophthalmol*. 2020;209:99−106.
8. Fan W, Uji A, Borrelli E, et al. Precise measurement of retinal vascular bed area and density on ultra-wide fluorescein angiography in normal subjects. *Am J Ophthalmol*. 2018;188:155−163.
9. Prasanna P, Bobba V, Figueiredo N, et al. Radiomics-based assessment of ultra-widefield leakage patterns and vessel network architecture in the PERMEATE study: insights into treatment durability. *Br J Ophthalmol*. 2021;105(8):1155−1160.
10. Ehlers JP, Wang K, Vasanji A, et al. Automated quantitative characterisation of retinal vascular leakage and microaneurysms in ultra-widefield fluorescein angiography. *Br J Ophthalmol*. 2017;101(6):696−699.
11. Ehlers JP, Jiang AC, Boss JD, et al. Quantitative ultra-widefield angiography and diabetic retinopathy severity: an assessment of panretinal leakage index, ischemic index and microaneurysm count. *Ophthalmology*. 2019;126(11):1527−1532.
12. Sevgi DD, Scott A, Patel SA, et al. Longitudinal assessment of quantitative ultra-widefield ischemic and vascular parameters in sickle cell retinopathy: exploratory evaluation of the geodesic diameter. *Invest. Ophthalmol. Vis. Sci*. 2020;61:3206.
13. O'Connell M, Sevgi DD, Srivastava SK, et al. Longitudinal precision of vasculature parameter assessment on ultra-widefield fluorescein angiography using a deep-learning model for vascular segmentation in eyes without vascular pathology. *Invest Ophthalmol Vis Sci*. 2020;61:2010.
14. Sevgi DD, Hach J, Srivastava SK, et al. Automated quality optimized phase selection in ultra-widefield angiography using retinal vessel segmentation with deep neural networks. *Invest Ophthalmol Vis Sci*. 2020;61:PB00125.
15. Sevgi DD, Scott AW, Martin A, et al. Longitudinal assessment of quantitative ultra-widefield ischaemic and vascular parameters in sickle cell retinopathy. *Br J Ophthalmol*. 2020 Oct 31. https://doi.org/10.1136/bjophthalmol-2020-317241. Online ahead of print.
16. Croft DE, van Hemert J, Wykoff CC, et al. Precise montaging and metric quantification of retinal surface area from ultra-widefield fundus photography and fluorescein angiography. *Ophthalmic Surg Lasers Imaging Retina*. 2014;45(4):312−317.
17. Legland D, Arganda-Carreras I, Andrey P. MorphoLibJ: integrated library and plugins for mathematical morphology with ImageJ. *Bioinformatics*. 2016;32(22):3532−3534.
18. Parsons-Wingerter P, Radhakrishnan K, Vickerman MB, Kaiser PK. Oscillation of angiogenesis with vascular dropout in diabetic retinopathy by VESsel GENeration analysis (VESGEN). *Invest Ophthalmol Vis Sci*. 2010;51(1):498−507.
19. Sambhav K, Abu-Amero KK, Chalam KV. Deep capillary macular perfusion indices obtained with OCT angiography correlate with degree of nonproliferative diabetic retinopathy. *Eur J Ophthalmol*. 2017;27(6):716−729.
20. Kim AY, Chu Z, Shahidzadeh A, et al. Quantifying microvascular density and morphology in diabetic retinopathy using spectral-domain optical coherence tomography angiography. *Invest Ophthalmol Vis Sci*. 2016;57(9):OCT362−OCT370.
21. Lee H, Lee M, Chung H, Kim HC. Quantification of retinal vessel tortuosity in diabetic retinopathy using optical coherence tomography angiography. *Retina*. 2018;38(5):976−985.
22. Sasongko MB, Wong TY, Nguyen TT, et al. Retinal vascular tortuosity in persons with diabetes and diabetic retinopathy. *Diabetologia*. 2011;54(9):2409−2416.
23. Patel V, Rassam S, Newsom R, et al. Retinal blood flow in diabetic retinopathy. *BMJ*. 1992;305(6855):678−683.
24. Jang Y, Jung HY, Hong Y, et al. Geodesic distance algorithm for extracting the ascending aorta from 3D CT images. *Comput Math Methods Med*. 2016;2016:4561979. https://doi.org/10.1155/2016/4561979.
25. Gui L, Tang X, Moura JMF. Geodesic distance on a Grassmannian for monitoring the progression of Alzheimer's disease. *Neuroimage*. 2017;146:1016−1024.